Efficient photonic reformatting of celestial light for diffraction-limited spectroscopy

D. G. MacLachlan,[1][⋆][†] R. J. Harris,[2][⋆][†] I. Gris-Sánchez,[3] T. J. Morris,[2] D. Choudhury,[1] E. Gendron,[4] A. G. Basden,[2] I. Spaleniak,[1] A. Arriola,[1] T. A. Birks,[3] J. R. Allington-Smith[2] and R. R. Thomson[1]

[1]*SUPA, Institute of Photonics and Quantum Sciences, Heriot–Watt University, Edinburgh EH14 4AS, UK*
[2]*Department of Physics, University of Durham, South Road, Durham DH1 3LE, UK*
[3]*Department of Physics, University of Bath, Claverton Down, Bath BA2 7AY, UK*
[4]*LESIA, Observatoire de Paris, Meudon, 5 Place Jules Janssen, F-92195 Meudon, France*

ABSTRACT

The spectral resolution of a dispersive astronomical spectrograph is limited by the trade-off between throughput and the width of the entrance slit. Photonic guided wave transitions have been proposed as a route to bypass this trade-off, by enabling the efficient reformatting of incoherent seeing-limited light collected by the telescope into a linear array of single modes: a pseudo-slit which is highly multimode in one axis but diffraction-limited in the dispersion axis of the spectrograph. It is anticipated that the size of a single-object spectrograph fed with light in this manner would be essentially independent of the telescope aperture size. A further anticipated benefit is that such spectrographs would be free of 'modal noise', a phenomenon that occurs in high-resolution multimode fibre-fed spectrographs due to the coherent nature of the telescope point spread function (PSF). We seek to address these aspects by integrating a multicore fibre photonic lantern with an ultrafast laser inscribed three-dimensional waveguide interconnect to spatially reformat the modes within the PSF into a diffraction-limited pseudo-slit. Using the CANARY adaptive optics (AO) demonstrator on the William Herschel Telescope, and 1530 ± 80 nm stellar light, the device exhibits a transmission of 47–53 per cent depending upon the mode of AO correction applied. We also show the advantage of using AO to couple light into such a device by sampling only the core of the CANARY PSF. This result underscores the possibility that a fully optimized guided-wave device can be used with AO to provide efficient spectroscopy at high spectral resolution.

Key words: instrumentation: adaptive optics – instrumentation: spectrographs.

1 INTRODUCTION

Spectrographs of unprecedented precision will be required to meet the ambitious science goals of modern astronomy in areas such as Earth-like exoplanet detection via the radial velocity technique (Mayor & Queloz 1995) and the Sandage test of the real-time rate of expansion of the Universe (Sandage 1962). To achieve the required precision, future spectrographs must operate at high spectral resolution ($R = \lambda/\mathrm{d}\lambda > 100\,000$), must be precisely calibrated, and must be exceptionally stable during any given measurement.

The requirement for high-precision spectrographs, operating efficiently on larger telescopes over a range of wavelengths, poses a variety of challenges to the design and construction of suitable spectrographs. For example, there tends to be a strong coupling between the size of a telescope and the size of the instruments required to efficiently process the light it captures. This coupling stems from equation (1), where it can be seen that the number of modes that form the point spread function (PSF) of a telescope scales with $(D_T/4\lambda)^2$ (Harris & Allington-Smith 2012; Spaleniak et al. 2013):

$$M \approx (\pi\, \theta_{\mathrm{Focus}} D_T/4\lambda)^2, \qquad (1)$$

where M is the number of modes that form the telescope PSF (for each polarization state), D_T is the diameter of the telescope, λ is the wavelength of the light, and θ_{Focus} is the angular width of the

PSF, obtained from a deconvolution of the diffraction-limited and seeing-limited images, but can be approximated as

$$\theta_{\text{Focus}} \approx \sqrt{(\lambda/D_{\text{T}})^2 + \theta_{\text{Seeing}}(\lambda)^2}, \tag{2}$$

where $\theta_{\text{Seeing}}(\lambda)$ is the so-called 'astronomical seeing' measured as the full width at half-maximum (FWHM) of the long-exposure PSF of the site in radians.

Equation (1) indicates that the number of modes that form a telescope PSF increases rapidly with increasing telescope aperture, and thus implies that larger telescopes require spectrographs with larger input slit-widths to maintain throughput (of course, this is assuming that the F-ratio of the optical input to the spectrograph is held constant). A larger slit-width then results in a larger spectrograph to maintain the required spectral resolution. The larger the instrument, the more expensive it is, and the lower the quality of the optics. The current generation of $\sim$8–10 m class telescopes already require appropriately scaled spectrographs, in order to obtain the desired resolving power with efficient input coupling, and future $\geq$30 m class extremely large telescopes would require even larger instruments (Cunningham 2009).

One approach to address the coupling between telescope size and spectrograph size implied by equation (1) is to employ adaptive optics (AO). A perfect AO system would, of course, produce a PSF that was diffraction-limited regardless of the size of the telescope. State-of-the-art extreme AO systems are now able to produce near-diffraction-limited PSFs (>90 per cent Strehl) on 8-m-class telescopes at near-infrared (near-IR) wavelengths in the H band, but only over a narrow field of view (Bailey et al. 2014; Close et al. 2014; Fusco et al. 2014; Jovanovic et al. 2014; Macintosh et al. 2014). It is also not yet clear how well AO systems will work on the new extremely large telescopes currently under construction: the European Extremely Large Telescope (E-ELT), the Thirty Metre Telescope (TMT), and the Giant Magellan Telescope (GMT), particularly at shorter wavelengths.

One approach that may complement AO systems, and enable the design of simpler and smaller spectrographs for larger telescopes, is the so-called PIMMS (photonic integrated multimode microspectrograph) concept (Bland-Hawthorn et al. 2010). The idea behind the PIMMS concept is to use a guided-wave transition, known as a 'photonic lantern' (Leon-Saval et al. 2005; Bland-Hawthorn et al. 2011; Thomson et al. 2011; Spaleniak et al. 2013; Birks et al. 2015), to efficiently couple the multimode telescope PSF to an array of single modes. These single modes can then be rearranged (or reformatted) into a linear array to form a pseudo-slit that acts as a diffraction-limited single-mode input (along the dispersion axis) to a spectrograph. Importantly, although the length of the slit in the PIMMS concept increases with increase in the number of modes in the PSF, the size of the spectrograph in the plane of dispersion is independent of the telescope size.

A further and potentially powerful benefit of the PIMMS concept is its potential to enable fibre-fed spectrographs which are precisely calibrated (Probst et al. 2015) and free of modal noise. Modal noise is a phenomenon present in multimode optical-fibre-fed spectrographs, where changes in the modal pattern at the output of the fibre effectively result in variations in the spectrograph linefunction (Lemke et al. 2011; McCoy et al. 2012). Interestingly, modal noise is expected to be completely absent in the single-mode regime, since the output of the fibre can exhibit only one spatial profile (neglecting polarization effects), is worst in the two-mode regime, and then becomes less severe due to statistical averaging as the number of modes in the fibre increases. If we assume that the fibre is designed to match the PSF, then equation (1) would imply that unless we are operating at the diffraction limit, using single-mode fibres, modal noise can become an increasing problem as the wavelength of operation increases, and/or AO systems improve. Modal noise has, for example, now been identified as being a critical issue in GIANO (Iuzzolino et al. 2014), a fibre-fed radial velocity spectrograph intended for operation at between 950 and 2500 nm on the 3.58-m Telescopio Nazionale Galileo (TNG). Under 0.6-arcsec seeing, the PSF of the TNG consists of $\sim$75 modes at 950 nm and just $\sim$12 modes at 2500 nm. Given these numbers, it is not at all surprising that the performance of GIANO is susceptible to significant modal noise issues.

It is important to note that polarization effects may also induce a novel form of modal noise, even in single-mode fibre-fed spectrographs. In this case, the instability is not the result of interference between spatial modes, but rather the result of polarization-dependent diffraction-efficiency profiles from the grating (Halverson et al. 2015). As suggested in Halverson et al. (2015), it should be possible to mitigate this phenomenon through mechanical agitation, although clearly this will require validation.

Previously, we have demonstrated that a fully integrated three-dimensional photonic device, which we named a 'photonic dicer' (MacLachlan et al. 2016a), could be used to reformat the multimode PSF from the CANARY AO system on the 4.2-m William Herschel Telescope (WHT) into a diffraction-limited pseudo-slit. The device, which was fully fabricated using an advanced laser manufacturing technique known as ultrafast laser inscription (ULI) (Davis et al. 1996; Jovanovic et al. 2012), seamlessly and monolithically integrated a photonic lantern transition with a spatial reformatting section. The device was tested on-sky by feeding the photonic dicer with H-band (1450–1610 nm) stellar light directly from CANARY, and was found to exhibit an on-sky throughput of 20 per cent (Harris et al. 2015), somewhat less than the 65 per cent measured in the laboratory due to suboptimal input coupling. Although this work proved the feasibility of using ULI-fabricated photonic reformatting components for applications in PIMMS-type instruments, for high-precision instruments, it will be highly desirable, if not essential, to decouple the instrument from the telescope slewing, in order to maximize the stability of the instrument. This will almost certainly be achieved using an optical-fibre feed to transport the light from the telescope focal plane to the spectrograph. One potential option to enable this would be to connect the photonic dicer to a standard multimode fibre, but recent work at Macquarie University has suggested that such an approach only induces a new form of modal noise that is due to strongly wavelength dependent coupling losses at the fibre–lantern interface (Cvetojevic et al., in preparation).

With the above issues in mind, an alternative approach is to use a multicore fibre (MCF) photonic lantern to collect the PSF from the telescope and use the MCF to transport the light from the telescope focal plane to the spectrograph. Such an approach has recently been implemented on the UK Schmidt telescope (Betters et al. 2014), where the two-dimensional array of modes generated by the MCF lantern was then fed directly into a compact spectrograph using the 'TIGER' approach (Leon-Saval, Betters & Bland-Hawthorn 2012; Betters et al. 2013). Unfortunately, as noted by Betters et al., the lantern used in this work was not correctly matched to the spectral range of the on-sky measurements, and the single-mode cores of the lantern were in fact few-moded at the measurement wavelength. Thus, the full capabilities of implementing photonic-lantern-enabled single-mode spectrographs on-sky, on an astronomical telescope, remain unproven.
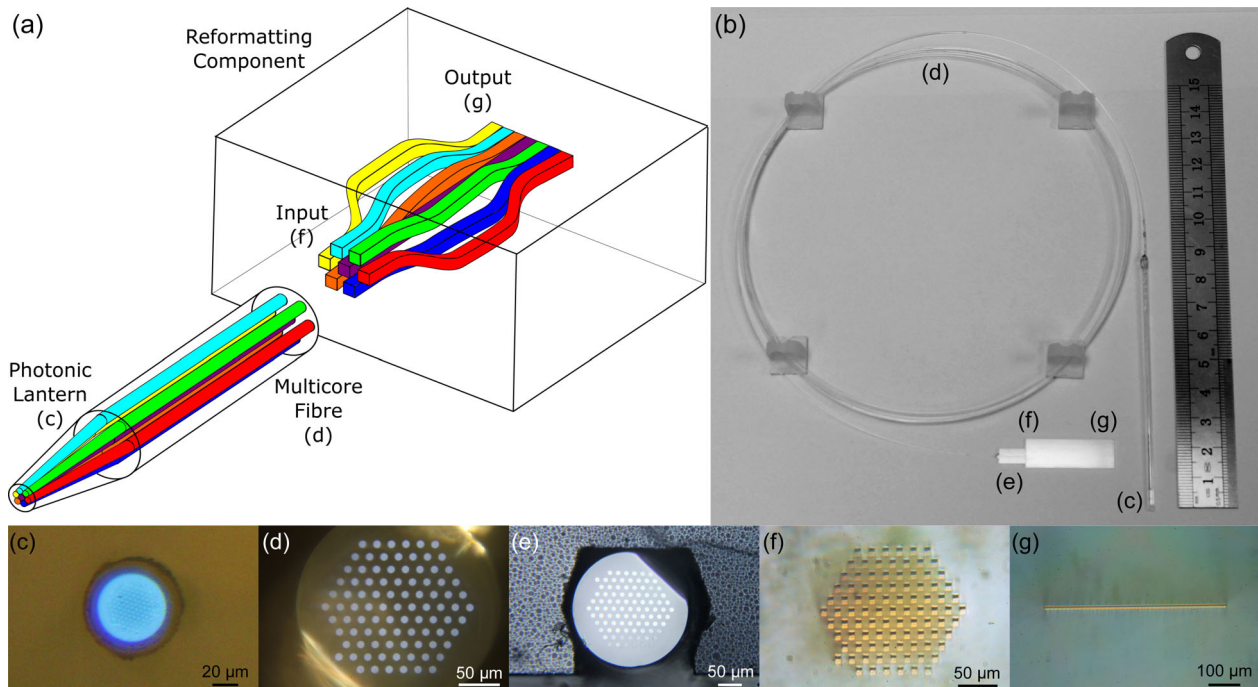
Figure 1. (a) 3D schematic of a simplified seven-core hybrid reformatter. The colours differentiate different waveguide paths. (b) Photograph of the hybrid reformatter device. (c) Photonic lantern with a multimode input port. (d) Facet of the multicore fibre, with the extra 92nd core visible in the bottom left-hand corner. (e) Multicore fibre placed in a custom ULI fabricated V-groove. (f) Input facet of the ULI manufactured reformatting component. (g) Pseudo-slit output of the reformatting component.

In this paper, we report the successful on-sky application of a 'hybrid' photonic-reformatter technology based on an MCF photonic lantern and a ULI fabricated reformatting component (Thomson et al. 2012) (Fig. 1) that reformats an AO-corrected *H*-band telescope PSF into a diffraction-limited pseudo-slit. The reformatting device presented here exhibited an on-sky throughput of 53 ± 4 per cent over a wavelength range of 1530 ± 80 nm, very close to the 65 per cent throughput measured in the laboratory over a wavelength range of 1550 ± 20 nm. We believe that such a hybrid approach, utilizing the key capabilities of both MCF photonic lanterns and 3D waveguide technologies, may enable compact high-resolution multimode spectrographs that operate at the diffraction limit and are free from modal noise.

Section 2 of this paper describes the design of the MCF lantern and the ULI fabricated component that form the hybrid reformatter. Section 3 provides a description of the experimental setup used for the on-sky test. Section 4 presents the results and analysis of the on-sky testing of both the hybrid reformatter and MCF lantern. Finally, Section 5 summarizes our findings and outlines our planned future work in this field.

2 HYBRID REFORMATTER DESIGN

We aimed to develop a hybrid device that could operate efficiently using the CANARY AO system, an on-sky AO demonstrator system (Myers et al. 2008) installed at the 4.2-m WHT in La Palma. To enable efficient operation, the hybrid reformatter must support at least the same number of modes as the number of modes that form the telescope PSF. The number of modes that form the CANARY PSF was calculated using equations (1) and (2). For our calculations, D_T is the diameter of the WHT (4.2 m). The central wavelength (λ) of our planned on-sky measurements was 1530 nm (Vidal et al. 2014), determined from the overlap between the passband of the *H*-band

filter and the responsivity of the Xenics Xeva-1.7 320 InGaAs camera used as a near-IR imager for the experiment. Under closed-loop operation (see Section 3), a typical AO-corrected PSF for the central wavelength in our experimental passband has a Strehl ratio of 20–30 per cent (Gendron et al. 2011). By considering the shortest wavelength within the FWHM of the passband ($\lambda = 1450$ nm), and CANARY operating in closed-loop mode providing an effective seeing of ≈ 0.465 arcsec in equation (1), the number of modes that form the AO-corrected PSF is ≈ 27. This is in contrast to the seeing-limited case, where the number of modes is ≈ 60, given median seeing at the WHT of 0.7 arcsec. Given these calculations, the hybrid reformatter was designed to support in excess of 60 orthogonal modes in order to ensure that efficient input coupling is maintained even under varying atmospheric seeing. We emphasize that the primary goal of this on-sky work was to clearly demonstrate that respectable on-sky throughputs can be achieved using hybrid devices of the type we have developed. In the future, hybrid reformatters will be specifically developed to match the PSF of the AO system in question, and thus take full advantage of the few-mode PSF generated by the system.

Figs 1(a) and (b) present a schematic and photograph of the hybrid reformatter. The fibre-optics section of the hybrid reformatter consists of a photonic lantern transition (Fig. 1c) formed from a multicore fibre (Fig. 1d). The core arrangement in our 92-core MCF was a centred hexagon of 91 cores (Fig. 1d), with a single additional core asymmetrically placed at the edge of the pattern as a marker to uniquely identify the orientation of the fibre, facilitating alignment with the ULI reformatter component. The MCF was made from fused silica, with step-index Ge-doped cores, using the standard stack and draw fibre fabrication technique. Each MCF core was 9 μm in diameter with a numerical aperture of 0.11. The adiabatic transition for the lantern was made by tapering the MCF in an F-doped capillary, as described in Birks et al. (2012, 2015), to form a

multimode input port with a core of cross-sectional diameter 43 μm and a numerical aperture of 0.22 (Fig. 1c). The input multimode core diameter was designed to support 92 modes, ensuring a low-loss transition with a throughput >89 per cent. The MCF was secured in a custom designed V-groove (Fig. 1e) in order to facilitate a secure connection to the ULI reformatting element.

The reformatting element of the hybrid reformatter was designed to match the 92 single modes generated by the MCF (Fig. 1f) and reformat them into a diffraction-limited pseudo-slit (Fig. 1g). For this purpose, the technique of ULI was used to directly inscribe (in the long axis) the reformatter inside the volume of a $30 \times 15 \times 1$ mm substrate of borosilicate glass (SCHOTT AF45; Meany et al. 2013). The fibre laser used for inscription emitted a 500-kHz train of 430-fs pulses at a wavelength of 1030 nm light. The waveguides were inscribed by focusing the laser light inside the substrate with a 0.4 numerical aperture aspheric lens. The substrate was translated through the laser focus at a speed of 8 mm s^{-1}, and each individual single-mode waveguide was constructed from 31 scans, with an interscan separation of 0.2 μm, in order to produce a ~6.2 μm wide area of positive refractive index modification. At the input end of the reformatter, 92 single-mode waveguides were arranged in a hexagonal geometry with a centre-to-centre separation of 17.6 μm (Fig. 1f), to match the measured core separation of the manufactured MCF. At the pseudo-slit end of the reformatter, the waveguides were arranged into a 1D array with a centre-to-centre separation of 6.2 μm and an overall length of ~ 570 μm (Fig. 1g). The throughput of each of the 92 reformatter waveguides was measured by injecting light using a standard SMF-28 fibre butt-coupled at the input with free-space coupling at the output. The 92 measurements were averaged to give a value of 75 ± 2 per cent for 1550-nm light, which represents the effective throughput of the reformatter component when the light is equally distributed between the waveguides. The pseudo-slit was single mode across the slit, with a mode field diameter of 8.4 μm at the $1/e^2$ point of a Gaussian fit. Given that the Numerical Aperture (NA) of a focused Gaussian beam is NA $\approx \lambda/(\pi\omega_0)$, where ω_0 is the $1/e^2$ radius of the beam waist, we estimate that the ULI waveguides exhibit a numerical aperture ≈ 0.12.

To assess the throughput performance of the ULI waveguides, a separate set of 30-mm-long straight waveguides was inscribed using the same parameters as those used to fabricate the waveguides in the reformatter. As expected, these straight waveguides were observed to be single mode in both axes at 1550 nm. By again using butt-coupling at the input and free-space coupling at the output, a throughput of 80 per cent was measured for the straight waveguides. We attribute the 5 per cent difference in throughput measured between the straight waveguides and the reformatter to the presence of waveguide bends in the latter.

The MCF lantern and ULI reformatter component were securely bonded with a UV-cured adhesive to form the hybrid reformatter. The throughput of the complete hybrid reformatter was tested in the laboratory over a wavelength of 1550 ± 20 nm to be 65 ± 2 per cent for incoherent multimode light. The polarization-dependent throughput of the reformatter was also measured to be 0.15 dB using 1548 nm laser light. As a final comment, it should also be noted that although the waveguides in this reformatter were brought together to form a single-mode slab waveguide at the output, we have recently reported (Spaleniak et al. 2016) that the different modes of the slab exhibit slightly different mode sizes and barycentres. This phenomenon is clearly not desirable for mode noise free spectrographs, and it may be necessary to reformat the modes into a linear array of uncoupled single modes in future devices to avoid this.

3 CANARY SETUP AND INTEGRATION

As CANARY is designed as an AO demonstrator, it can be configured to many different modes of correction (Myers et al. 2008). In this case, the system was configured to provide closed-loop AO correction using an on-axis natural guide star as a wavefront reference. A dichroic mirror transmits light > 1000 nm to the experiment with visible wavelengths reflected to a 36 subaperture Shack–Hartmann wavefront sensor (WFS). A fast-steering mirror and 52-actuator deformable mirror (DM) are driven by the WFS measurements, providing a partially corrected PSF at a wavelength of 1500 nm. A basic integrator feedback controller with a closed-loop gain of 0.3 was used to calculate the DM commands, with the WFS positioned behind the DM measuring the residual wavefront error after correction.

Alignment and optimization of the experimental system (Fig. 2) was performed during the day using a range of sources available in the CANARY setup. In our case, a 1550-nm laser beam coupled into a single-mode fibre was moved into the CANARY input focal plane, passed through the entire CANARY optical train, and the PSF reimaged on to the multimode input at the photonic-lantern end of the hybrid reformatter. The surface shape of the DM was modified by engaging the AO-correction loop and artificially applying static offset terms to the measured WFS signal. These offsets were automatically adjusted using the Nelder–Mead simplex method (Nelder & Mead 1965) to alter the PSF shape at the hybrid reformatter input and maximize the detected flux from its pseudo-slit output. The optimum measured wavefront values and corresponding DM shape were recorded and used as the correction reference for on-sky tests.

To investigate the effect of different degrees of AO correction on the hybrid reformatter, CANARY was operated in three modes. Closed-loop mode provides the maximum degree of correction achievable, where both tip-tilt and higher order wavefront aberrations were corrected with an update rate of 150 Hz. In tip-tilt mode, the high-order AO correction of the optimized PSF shape is removed by reducing the integrator loop gain to a low value (typically 0.001), with the PSF location simply stabilized in real time. Open-loop mode applies the minimum correction of the three modes of operation by additionally reducing the tip-tilt correction gain. This allowed the PSF to remain in the reference location for optimum coupling but without high temporal frequency correction.

As shown in Fig. 2, the on-sky experimental setup comprised two science arms and a separate reference arm. A beamsplitter (BS1) was used to direct ~10 per cent of the light within the CANARY PSF to the reference arm, where a lens (L7) formed an image of the PSF on to the InGaAs camera. The reference arm enabled the shape and photon flux within the PSF to be 'self-referenced' during observation, allowing the transmission of the hybrid reformatter to be measured regardless of variations in the PSF. A 0.6 absorptive neutral density filter (ND) was placed in this arm to ensure that the camera pixels did not saturate during data acquisition. An *H*-band spectral filter (F) was mounted at the entrance to the camera. A second beamsplitter (BS2) was introduced to direct ~81 per cent of the remaining light into the secondary science arm, where it was injected into the multimode end of a second MCF photonic lantern (which we will call the secondary lantern) using lens L4. The final ~9 per cent of the light in the primary science arm was coupled into the hybrid reformatter using lenses L2 and L3. The output ends of the secondary lantern and hybrid reformatter were adjacently positioned in the vertical axis such that both could be imaged through lenses L5 and L6 on to the camera simultaneously. The detector response of the InGaAs camera was measured in the
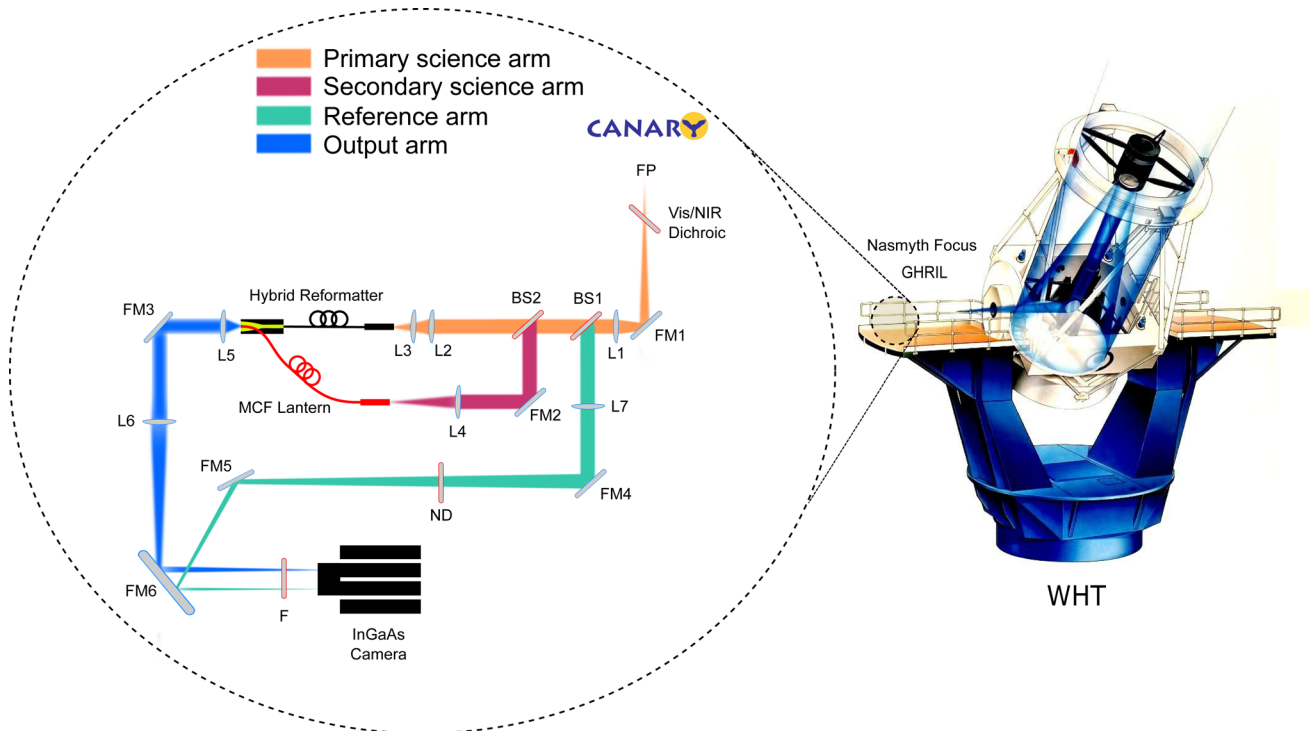
Figure 2. Schematic diagram showing the free-space optical setup used for the on-sky tests. Stellar light collected by the WHT is fed through the CANARY AO system, which generates a corrected multimode PSF. A dichroic is used to remove the visible part of the spectrum (<1000 nm) from the light beam, which is then collimated using a lens (L1). Using a beamsplitter (BS1), 10 per cent of the collimated beam is fed to a reference path containing a 0.6 absorptive neutral density filter (ND), and re-imaged the PSF on to the camera using L7. The remaining light passes through another beamsplitter (BS2), which reflects 81 per cent to the secondary science arm. The light in this arm is focused by L4 and allows the core of the PSF to be imaged on to the multimode port of the secondary lantern. The rest of the light is focused by L2 and L3 on to the hybrid reformatter, which samples the whole PSF. The reformatted output from both the hybrid reformatter and secondary MCF lantern are imaged on to the camera using lenses L5 and L6. The fold mirrors (FM1–FM6) are utilized for beam steering. An *H*-band spectral filter (F) was placed at the entrance to the camera. (WHT image courtesy of the Isaac Newton Group of Telescopes, La Palma).

laboratory using a 1550-nm light-emitting diode with a calibrated integrating sphere detector and found to be linear to within $\ll 1$ per cent over the signal levels used throughout the experiments.

CANARY provides an $\approx$F/11 beam with a plate scale value of 4.54 arcsec mm^{-1}, but this is obviously altered by the input coupling optics in the two arms (L2 to L4 in Fig. 2). The scaling of each arm was measured by taking images at the focus of each arm while translating an IR source at another known focal plane within CANARY. The primary science arm was designed to couple the entire PSF, with an F/2.29 $\pm$ 0.28 beam and a plate scale of 21.8 $\pm$ 1.34 arcsec mm^{-1}. This means that the hybrid reformatter input had an angular size of 1.1 $\pm$ 0.07 arcsec. The secondary science arm was designed to couple the core of the PSF, with an F/11.07 $\pm$ 0.32 beam and a plate scale of 4.57 $\pm$ 0.13 arcsec mm^{-1}. This means that the secondary MCF lantern input had an angular size of 0.23 $\pm$ 0.01 arcsec.

For each mode of AO operation, multiple data sets were acquired, where each data set comprised 100 near-IR images. The camera exposure time for each image was 400 ms. The background noise floor was determined through dark exposures and periodically acquiring data sets of sky background images. After acquiring an adequate number of data sets, the hybrid reformatter and secondary lantern were removed from the primary science arm, and the lens L5 was translated towards lens L3 such that the PSF could be imaged directly on to the camera through the primary science arm. Additional data sets of 100 images were acquired in order to calibrate the instrument for the difference in the integrated power between the

reference and primary science arms. This allowed the throughput of the hybrid reformatter to be calibrated using the star itself.

4 RESULTS

The hybrid reformatter and the secondary lantern were tested on-sky at the WHT on 2014 October 11 and 12, with all data acquired between 20:30 and 22:45 GMT. The star selected for observation was TYC 3156-2223-1 (Gamma Cygni) from the Tycho 2 catalogue (Hog et al. 2000), a first magnitude star in the astronomical *H* band. The astronomical seeing values, as measured using an on-site monitor (O'Mahoney 2003), varied between 0.5 and 0.8 arcsec over the course of the measurements, representative of median seeing for the telescope site.

Fig. 3 shows the near-IR images for each AO mode and results from the corresponding throughput evaluation using data acquired on the night of 2014 October 11. The images presented here (Fig. 3, top row) have been averaged over 100 frames and show the pseudo-slit and secondary lantern outputs that were imaged on to the camera using the primary science arm, as well as the CANARY PSF, which was imaged using the reference arm (see Fig. 2). The imperfect cleave forming the multicore end of the secondary lantern can also be seen in the images. In the case of closed-loop operation with full AO correction, the transmission of the hybrid reformatter was measured to be 53 $\pm$ 4 per cent. With a reduced degree of atmospheric correction, the device transmission was measured to be 47 $\pm$ 5 and 48 $\pm$ 5 per cent in the case of tip-tilt and open-loop operations,
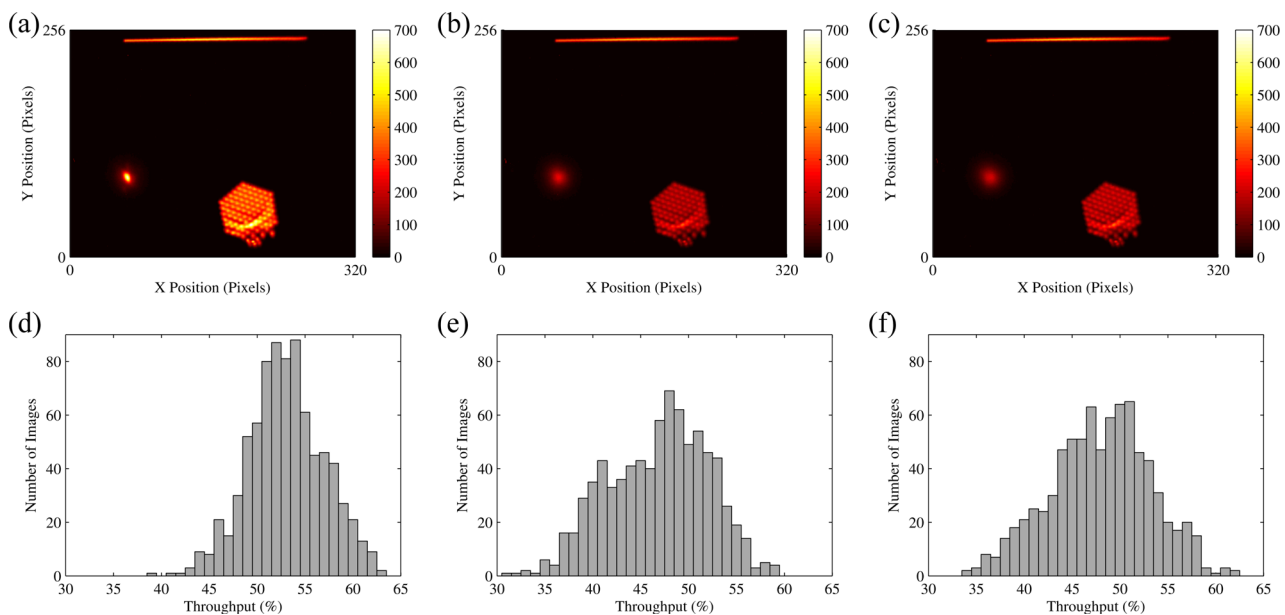
Figure 3. Colour map images of the camera sensor for averaged, reduced data showing the output of the hybrid reformatter (along the very top), the secondary lantern (lower right-hand side), and the telescope PSF (lower left-hand side) from the reference path for (a) closed-loop, (b) tip-tilt only, and (c) open-loop modes of AO correction. Note: The camera has 30 μm pixels and the secondary lantern output is distorted due to an imperfect cleave. Bottom row: histogram plots showing the percentage transmission distribution over the number of images acquired for (d) closed-loop, (e) tip-tilt, and (f) open-loop AO modes. Hot pixel removal and background correction algorithms have been applied prior to evaluating the transmission for each image frame acquired.

respectively. Histograms of the transmission data obtained for the respective AO modes are shown in Fig. 3 (bottom row).

For experiments conducted on the night of 2014 October 12, the multicore end of the secondary lantern was recleaved to produce an improved image on the camera. As the experimental design did not allow for easy calibration of a reference PSF image to be obtained in the secondary science arm, the absolute throughput of the secondary lantern was not determined. Nonetheless, comparative measurements between the closed-loop and tip-tilt modes of AO operation were performed. These were taken in the same manner as the throughput measurements, with the calculated closed-loop and tip-tilt flux divided to provide a ratio of the two. These measurements revealed an averaged flux ratio of 2:1, which is much lower than that expected, according to the area of the sampled PSF in both cases. To examine this discrepancy, an on-sky dither was performed, whereby the tip-tilt mirror in the CANARY setup was used to move the PSF by ± 1.25 arcsec relative to the inputs of the hybrid reformatter and the secondary lantern, which have an effective angular size of 1.1 and 0.23 arcsec, respectively.

Fig. 4 shows the results of the dither experiments for the respective devices, with each square representing the total flux of the tested device for each PSF position. The centre of each plot shows the location (in arcsec) of the centre of the PSF as set on the bench, with the black circles representing the respective angular size of the device input. The dither plots clearly show that the actual area of maximum flux does not overlap with the expected area. This mismatch can be attributed to atmospheric refraction causing a chromatic shift between the corrected (visible guide star) path and the science (near-IR) path and will be corrected in future experimentation.

It can also be seen from Fig. 4 (middle column) that the hybrid reformatter is relatively insensitive to the dither position in both closed-loop and tip-tilt operating modes, with closed-loop correction providing approximately 35 per cent improvement over tip-tilt

correction at the optimum input position. The secondary lantern (Fig. 4, right-hand column) is also insensitive in tip-tilt mode, though highly sensitive in closed-loop mode and demonstrates approximately 58 per cent improvement in throughput between closed-loop and tip-tilt correction. It should be noted that the dithers did not incorporate the simplexing routine that was applied during the throughput demonstration of the previous night, and so were not fully optimized for off-axis positions.

5 CONCLUSIONS

We have presented results from the on-sky tests of a photonic guided-wave device that spatially reformats an AO corrected telescope PSF into a diffraction-limited pseudo-slit. This hybrid reformatter integrates a low-loss MCF photonic lantern that adiabatically converts the modes within the PSF into a 2D array of single modes, with a ULI fabricated reformatter component that spatially rearranges the single modes into a pseudo-slit waveguide that is single mode in the dispersion axis. Our aim is that devices based on this concept will convert any modal noise into amplitude and phase variations orthogonal to the dispersion axis of an instrument following improvements to the output array, and could enable high-resolution, high-stability spectrographs operating on large telescopes, or in situations where modal noise is a severe issue. The calibration tools and controls required to optimize coupling to an AO system were developed and the device performance tested for a range of modes of AO operation. The maximum on-sky throughput achieved was 53 ± 4 per cent, while the in-laboratory throughput was measured to be 65 ± 2 per cent. This performance demonstrates a significant improvement over that achieved in our earlier demonstration of the fully integrated ULI reformatter (the photonic dicer).

To conclude, we believe that the results presented here highlight the potential of efficiently implementing guided-wave reformatting devices in astronomy, specifically for coupling multimode light to
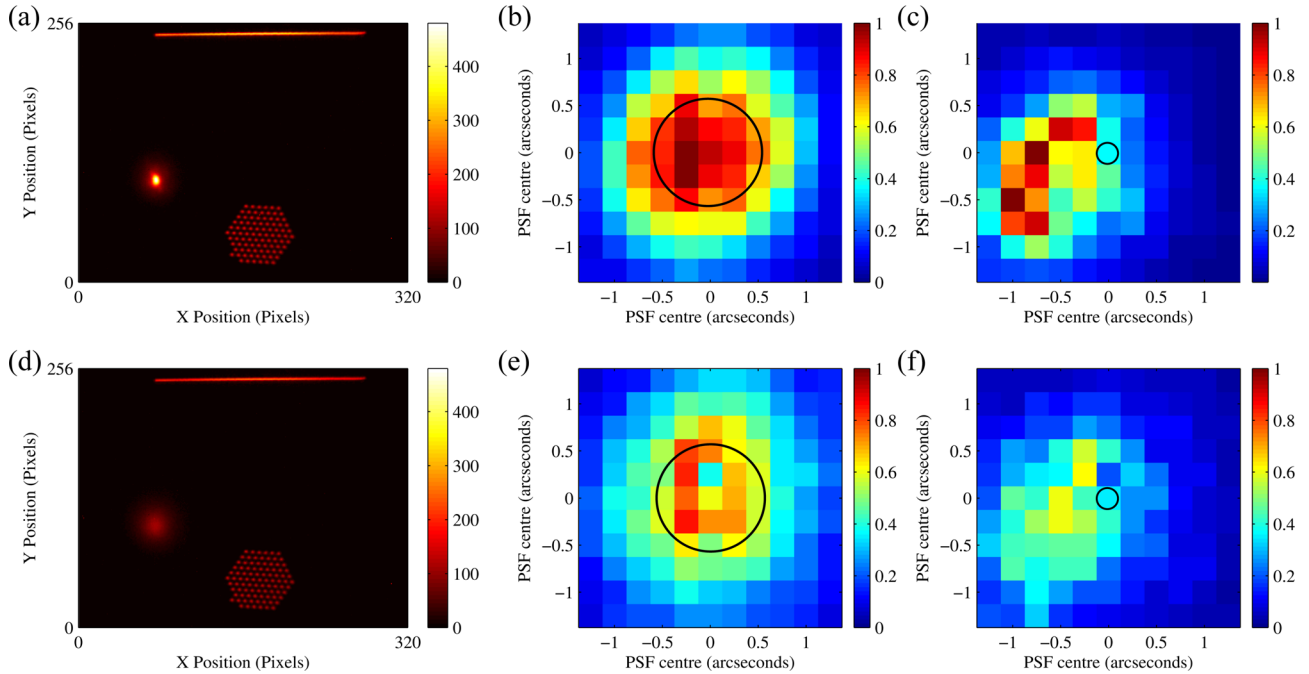
Figure 4. Dither plots for the night of 2014 October 12. The top row shows closed-loop operation and the bottom row shows tip-tilt operation. The left-hand column shows averaged reduced data obtained from the camera. The middle column images show the position of the dithered PSF, with the colour bar being normalized flux for the slit of the hybrid reformatter. The right-hand column images show the position of the dithered PSF, with the colour bar being normalized flux for the secondary photonic lantern. The black circles represent the angular size of the input fibre in each science arm.

spectrographs operating at the diffraction limit. This approach may have important applications in many areas such as radial velocity measurements and exoplanet atmospheric spectroscopy.

Data

Raw experimental data are available on the Heriot–Watt PURE system (MacLachlan et al. 2016b).

REFERENCES

Bailey V. P. et al., 2014, in Marchetti E., Close L. M., Véran J.-P., eds, Proc. SPIE Conf. Ser. Vol. 9148, Adaptive Optics Systems IV. SPIE, Bellingham, p. 914803

Betters C. H., Leon-Saval S. G., Robertson J. G., Bland-Hawthorn J., 2013, Opt. Express, 21, 26103

Betters C. H., Leon-Saval S. G., Bland-Hawthorn J., Richards S. N., Birks T. A., Gris-Sánchez I., 2014, in Ramsay S. K., McLean I. S., Takami H., eds, Proc. SPIE Conf. Ser. Vol. 9147, Ground-Based and Airborne Instrumentation for Astronomy V. SPIE, Bellingham, p. 91471I

Birks T. A., Mangan B. J., Díez A., Cruz J. L., Murphy D. F., 2012, Opt. Express, 20, 13996

Birks T. A., Gris-Sánchez I., Yerolatsitis S., Leon-Saval S. G., Thomson R. R., 2015, Adv. Opt. Photonics, 7, 107

Bland-Hawthorn J. et al., 2010, in McLean I. S., Ramsay S. K.; Takami H., eds, Proc. SPIE Conf. Ser. Vol. 7735, Ground-Based and Airborne Instrumentation for Astronomy III. SPIE, Bellingham, p. 77350N

Bland-Hawthorn J. et al., 2011, Nature Commun., 2, 581

Close L. M. et al., 2014, in Marchetti E., Close L. M., Véran J.-P., eds, Proc. SPIE Conf. Ser. Vol. 9148, Adaptive Optics Systems IV. SPIE, Bellingham, p. 91481M

Cunningham C., 2009, Nature Photonics, 3, 239

Davis K. M., Miura K., Sugimoto N., Hirao K., 1996, Optics Lett., 21, 1729

Fusco T. et al., 2014, in Marchetti E., Close L. M., Véran J.-P., eds, Proc. SPIE Conf. Ser. Vol. 9148, Adaptive Optics Systems IV. SPIE, Bellingham, p. 91481U

Gendron E. et al., 2011, A&A, 529, L2

Halverson S., Roy A., Mahadevan S., Schwab C., 1995, ApJ, 814, L22

Harris R. J. Allington-Smith J. R., 2012, MNRAS, 428, 3139

Harris R. J. et al., 2015, MNRAS, 450, 428

Hog E. et al., 2000, A&A, 355, L27

Iuzzolino M., Tozzi A., Sanna N., Zangrilli L., Oliva E., 2014, in Ramsay S. K., McLean I. S., Takami H., eds, Proc. SPIE Conf. Ser. Vol. 9147,

Ground-based and Airborne Instrumentation for Astronomy V. SPIE, Bellingham, p. 914766

Jovanovic N. et al., 2012, MNRAS, 427, 806

Jovanovic N. et al., 2014, in Ramsay S. K., McLean I. S., Takami H., Proc. SPIE Conf. Ser. Vol. 9147, Ground-Based and Airborne Instrumentation for Astronomy V. SPIE, Bellingham, p. 91471Q

Lemke U., Corbett J., Allington-Smith J. R., Murray G., 2011, MNRAS, 417, 689

Leon-Saval S. G., Birks T. A., Bland-Hawthorn J., Englund M., 2005, Opt. Lett., 30, 2545

Leon-Saval S. G., Betters C. H., Bland-Hawthorn J., 2012, in Navarro R., Cunningham C. R., Prieto E., eds, Proc. SPIE Conf. Ser. Vol. 8450, Modern Technologies in Space- and Ground-Based Telescopes and Instrumentation II. SPIE, Bellingham, p. 84501K

Macintosh B. A. et al., 2014, in Marchetti E., Close L. M., Véran J.-P., eds, Proc. SPIE Conf. Ser. Vol. 9148, Adaptive Optics Systems IV. SPIE, Bellingham, p. 91480J

MacLachlan D. G., Harris R. J., Choudhury D., Simmonds R. D., Salter P. S., Booth M. J., Allington-Smith J. R., Thomson R. R., 2016a, Opt. Lett., 41, 76

MacLachlan D. G. et al., 2016b, Experimental Data. Available at: http://doi.org/10.17861/a2ffabae-a30a-46df-b020-bf8f80664c7e

Mayor M., Queloz D., 1995, Nature 378, 355

McCoy K. S., Ramsey L., Mahadevan S., Halverson S., Redman S. L., 2012, in McLean I. S., Ramsay S. K., Takami H., eds, Proc. SPIE Conf. Ser. Vol. 8446, Ground-Based and Airborne Instrumentation for Astronomy IV. SPIE, Bellingham, p. 84468J

Meany T., Gross S., Jovanovic N., Arriola A., Steel M. J., Withford M. J., 2013, Appl. Phys. A, 114, 113

Myers R. M. et al., 2008, in Hubin N., Max C. E., Wizinowich P. L., eds, Proc. SPIE Conf. Ser. Vol. 7015, Adaptive Optics Systems. SPIE, Bellingham, p. 70150E

Nelder J. A., Mead R., 1965, Comput. J. 7, 308

O'Mahoney N., 2003, Newsl Isaac Newton Group Telesc., 7, 22

Probst R. A. et al., 2015, New J. Phys., 17, 023048

Sandage A., 1962, AJ, 136, 319

Spaleniak I., Jovanovic N., Gross S., Ireland M. J., Lawrence J. S., Withford M. J., 2013, Opt. Express, 21, 27197

Spaleniak I., MacLachlan D. G., Gris-Sánchez I., Choudhury D., Harris R. J., Allington-Smith J. R., Birks T. A., Thomson R. R., 2016, in Navarro R., Burge J. H., eds, Proc. SPIE Conf. Ser. Vol. 9912, Advances in Optical and Mechanical Technologies for Telescopes and Instrumentation II. SPIE, Bellingham, p. 991228

Thomson R. R., Birks T. A., Leon-Saval S. G., Kar A. K., Bland-Hawthorn J., 2011, Opt. Express, 19, 5698

Thomson R. R., Harris R. J., Birks T. A., Brown G., Allington-Smith J., Bland-Hawthorn J., 2012, Opt. Lett., 37, 2331

Vidal F. et al., 2014, A&A, 569, A16

This paper has been typeset from a TeX/LaTeX file prepared by the author.